

Chapter 17

Power Grid Time Synchronization for Phase-Sensitive Vibration Measurements



Ferrill T. Rushton, Eugene H. Lin, Jessica Y. Chan, Adam J. Wachtor, Eric B. Flynn, and Nick Lieven

Abstract Phase-sensitive vibration measurements, such as those used for modal analysis, require precise time synchronization between sensors. However, current time synchronization approaches often require specialized hardware and may be impractical to use in certain environments. For example, global positioning system (GPS) synchronization requires GPS receivers and line of sight to GPS satellites, making it difficult to implement such systems underground or indoors.

This paper proposes a new solution for time synchronization that takes advantage of the frequency fluctuations in the power grid. The United States (US) power grid operates at a nominal frequency of 60 Hz and is comprised of three interconnections. However, the actual frequency varies by tens of millihertz over the course of a minute. If measured simultaneously with sensors of interest, this variation provides a basis for signal-based synchronization. These fluctuations are simultaneously observed at any point within an interconnection, allowing the time delay estimation to compare signals from different sensors.

This paper compares the accuracy of the power grid time synchronization to traditional synchronization methods using a free-free beam test performed with accelerometers connected to different data acquisition devices (DAQs), which in turn were connected to the power grid. The raw data was time synchronized using various synchronization approaches and the first three operating deflection shapes of the beam were compared. Results show that power grid time synchronization is able to determine operating deflection shapes as accurately as other traditional synchronization methods. As a result, power grid time synchronization is a viable solution for synchronizing sensors for phase-sensitive vibration measurements where other synchronization methods are infeasible or too expensive.

Keywords Phase-sensitive vibration measurements · Modal analysis · Time synchronization · Power grid · Time delay estimation

17.1 Introduction

Time sensitive vibration experiments, such as those involved in structural health monitoring [1], modal analysis, and wave propagation, are vital to monitoring structures and their structural properties. However, depending on the type of structure and operational environment, difficulties may arise in associating the correct times to the respective measurements accurately. In localized vibration measurements, sensors can be connected to the same DAQ unit, thus inherently providing time synchronization. However, if the sensors are distributed over a large spatial domain, connecting them to the same DAQ

This work was performed during the 2019 Los Alamos Dynamics Summer School at Los Alamos National Laboratory.

F. T. Rushton · E. H. Lin · J. Y. Chan
University of California, San Diego/La Jolla, CA, USA
e-mail: frushton@ucsd.edu; ehlin@ucsd.edu; jyc125@ucsd.edu

A. J. Wachtor (✉) · E. B. Flynn
Los Alamos National Laboratory, Los Alamos, NM, USA
e-mail: ajw@lanl.gov; eflynn@lanl.gov

N. Lieven
University of Bristol, Bristol, UK
e-mail: Nick.Lieven@bristol.ac.uk

is sometimes not practical and often infeasible. As a result, different time synchronization approaches must be applied between DAQs. However, time synchronization approaches are not as accurate as a direct shared connection, and different applications have requirements which are not always possible [2]. For example, in the case of GPS synchronization [3], GPS receivers need line of sight to GPS satellites, which often greatly increases experimental complexity when trying to implement systems underground or within buildings. As another example, wired networks may not be possible when physical barriers exist between sensors. In an attempt to provide an alternative approach, this study explores the use of unique fluctuations of the US power grid's nominal frequency to time-synchronize sensors on spatially distributed DAQs that are designed for vibrational measurements.

There are several considerations which are relevant to time synchronization of sensors via the power grid which include:

1. Understanding why the power grid frequency fluctuates from the nominal frequency of 60 Hz;
2. Which time-delay estimation techniques should be used to align out-of-phase signals from different sensors;
3. Resolving misalignment of clocks on different DAQs; and
4. Verifying that power grid synchronization provides the accuracy needed for phase sensitive vibration measurements by comparing power grid time synchronization experimental results with the results acquired from traditional time synchronization techniques.

17.2 Background

17.2.1 Power Infrastructure

The US power grid is separated into three different interconnections, Eastern, Western, and Texas, each of which consists of one or more balance authorities (BAs). The BAs are responsible for predicting power demands based on a combination of historical data, seasonal demand, and weather forecasts. Depending on the demand, one BA will coordinate with another BA to intentionally create a power imbalance between the two BAs by increasing power generation at the first BA relative to the second BA to facilitate the transfer of electricity between the two BAs. The transfer of electricity will change the supply in the power grid. In addition to the supply changing within the power grid, the demand also changes throughout the day.

The combination of continuous changes in supply and demand throughout the day creates changes in the nominal 60 Hz frequency of the US power grid. When supply is greater than demand, the frequency is greater than 60 Hz. Likewise when demand is greater than supply, the frequency is less than 60 Hz [4, 5]. The variation from the nominal power grid frequency of 60 Hz provides a unique time signature that can be used for time synchronization between two or more spatially distributed sensors [6]. Furthermore, for power to be delivered efficiently across the country, the phase difference between any two points should be approximately constant, so the power grid is phase-coherent [7].

17.2.2 Modal Analysis

Modal analysis is one method of measuring a structure's properties using vibration measurements. Modal analysis is the study of a structure's characteristics or dynamic properties which includes natural frequencies, damping ratios, and mode shapes. Generally, a structure has multiple modes in different amplitudes, and the combination of these amplitudes of frequencies create a general frequency response function (FRF) that will be analyzed [8]. A structure's state can be assessed using modal analysis and then controlled using the assessment [9].

Modal analysis captures the linear input-output relationship between points on a structure. Mode shapes and operating deflection shapes (ODS), which represent the spatial distribution, are derived from measures of the relative phase at each point. As a result, modal analysis is a phase-sensitive vibration measurement technique and thus requires accurate time synchronization in order to produce meaningful results.

Experimental modal tests are generally conducted with either an impact test, or a shaker test. Impact testing involves tapping the structure with a hammer at prescribed locations, while shaker testing involves shaking the structure on a test table at a set of frequencies. Impact testing is easy and portable, while shaker testing allows for a more controllable excitation of the tested structure [8].

In order to determine the accuracy of the mode shapes extracted, the modal assurance criterion (MAC) is used. The MAC is a vector correlation tool developed to check the similarity between two different modal vectors. When MAC diagonal

values are closer to one, it means the two corresponding modal vectors are correlated. When MAC diagonal values are closer to zero, it means the two vectors are uncorrelated [8].

17.2.3 Time Synchronization

Time synchronization is vital to an accurate phase-sensitive vibration experiment. Time synchronization allows the data from one sensor to be collected at the same time and rate as that from another, which in turn makes it possible to pinpoint which data points correspond to which events. This involves reference clocks and sample clocks. Reference clocks are generated to be referenced by other clocks. Sample clocks are used to dictate the timing of the recording of samples from a signal. Reference clocks are generated so that a sample clock can record data between devices synchronously. Of the several issues that arise in an experiment that requires time synchronization, the two main issues are clock drift and clock skew. Clock skew is where clocks start at different times, which results in misaligned timing information. Clock drift is where clock sampling frequencies begin to drift apart due to inaccuracies in each of their clocks [10]. Both of these issues are tackled in different ways in various time synchronization approaches mentioned in the next section.

17.2.4 Time Synchronization Approaches

There are many approaches to the problem of time synchronization, with a number of unique solutions developed in recent years. These approaches fall generally under two categories, time-based synchronization and signal-based synchronization. In time-based synchronization, DAQ units align their clocks to a common time source. In signal-based synchronization, the clocks and trigger signals are shared between two DAQ units [11].

One of the most popular approaches uses the GPS. This is a time-based synchronization approach where DAQ units reference a GPS time source. Synchronizations within 100 ns of UTC can be readily achieved if delays of equipment are accounted for (i.e. receiver, antenna, antenna cable, etc). The cost of implementing a GPS time synchronization system varies greatly depending on the accuracy needed [12], but all such systems require specialized equipment. Furthermore, all GPS receivers must have a clear line-of-sight to reliably measure signals from the satellites, making a GPS-based time synchronization system ill-suited for underground, indoors, and obstructed-view environments [13].

In recent years, work has been done to time synchronize systems using other external sources. Li et al., 2011, took advantage of periodic pulses in FM broadcasts by utilizing FM receiver hardware integrated with ROCS (RDS-assisted cLock Calibration for SensorNet) for time-synchronization [14]. Hao et al., 2014, use an 802.15.4 sensor to detect and synchronize to the periodic beacons broadcasted by Wi-Fi access points with an average synchronization error of 0.12 ms over a period of 10 days [7, 15]. Li et al., 2012, also indirectly exploit the power grid by measuring the intensity changes of fluorescent lights, which form a stable period equal to half that of the power grid's [16]. The last work we discuss in this paper comes from Viswanathan et al., 2016. Viswanathan et al. take advantage of the fluctuations of the power grid from its nominal frequency (i.e. 60 Hz in the United States and 50 Hz in Europe) by using specialized hardware (MCU with sampling rate of 4.2 MHz) to find zero-point crossings to estimate AC cycle lengths. They show that the fluctuations in the nominal frequency of the power grid ensure that, given a sufficient length of time, a unique "Time Fingerprint" (TiF) can be acquired. A TiF from one node, along with its timestamp, can be compared to the "history" of another node to find the time offset between the two nodes' clocks [6].

These approaches all have certain drawbacks. A number of them [6, 7, 14] require specialized hardware, increasing the difficulty and cost of implementing such a time-synchronization approach. Hao et al., 2014, requires the use of an 802.15.4 sensor [15], and Li et al., 2012, require the use of a light sensor [16]. This equipment may not already be implemented in a system. There are other specific drawbacks, such as the susceptibility of equipment to interference from electromagnetic radiation [7]. As another example, the flickering fluorescent light approach requires fluorescent lighting, so is ill-suited for dark environments or outside applications. Lastly, in general, these approaches do not readily allow for retroactive time synchronization of data from a generic data acquisition environment. The method proposed in this paper utilizes pre-existing acquisition equipment typically associated with vibration measurements.

17.2.5 Time-Delay Estimation (TDE) Techniques

In order to synchronize the clock skew between DAQ units, time delay estimation must be performed to align signals. An abundance of TDE techniques exist in published literature. The factors that need to be considered when selecting a TDE technique to implement are as follows [17]:

- Signal to Noise Ratio (SNR)
- Type of input signal (i.e. input step signal)
- Estimation accuracy required
- The size of the sampling period in comparison to the time-delay length

One of the simplest TDE techniques is cross-correlation. Mathematically, the cross-correlation is defined as the following (Eq. 17.1) [18]:

$$w(t) = u(t) \otimes v(t) \triangleq \int_{-\infty}^{\infty} u^*(\tau) v(\tau + t) d\tau \quad (17.1)$$

Where the symbol \otimes represents the cross-correlation operator, $u(t)$ and $v(t)$ are two signals, and $w(t)$ can provide a measure of the “lag” between $u(t)$ and $v(t)$. The maximum value of $w(t)$ is the most likely time-delay between the two signals, i.e. at the time-delay where the signals best match up, the value of the integral is maximized. As illustrated in Fig. 17.1, if the maximum value of $w(t)$ is 450 ms, then the value of $u(\tau)$ is the same as the value of $v(\tau + 450)$ [18].

17.2.6 Time Synchronization Requirements for Vibration Measurements

Time Synchronization is vital to a well conducted vibration measurement. Without time synchronization, data is misaligned and the coherence is lowered, reducing the accuracy of the experiment. Time synchronization is dependent on the sampling frequency of the experiment. The lower the sampling frequency, the lower the need for precise time synchronization. For example, when a vibration experiment on a laboratory floor was sampled at 100 Hz, the modes were correctly identified when using low precision synchronization methods [19]. However, if the vibration experiment is interested in higher frequencies, a higher sampling frequency is necessary, requiring more precision.

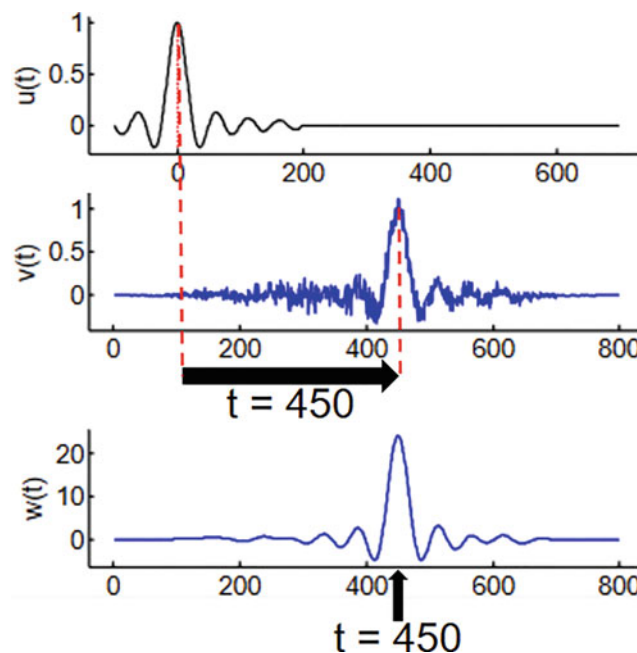


Fig. 17.1 Cross-correlation between $u(t)$ and $v(t)$ [18]

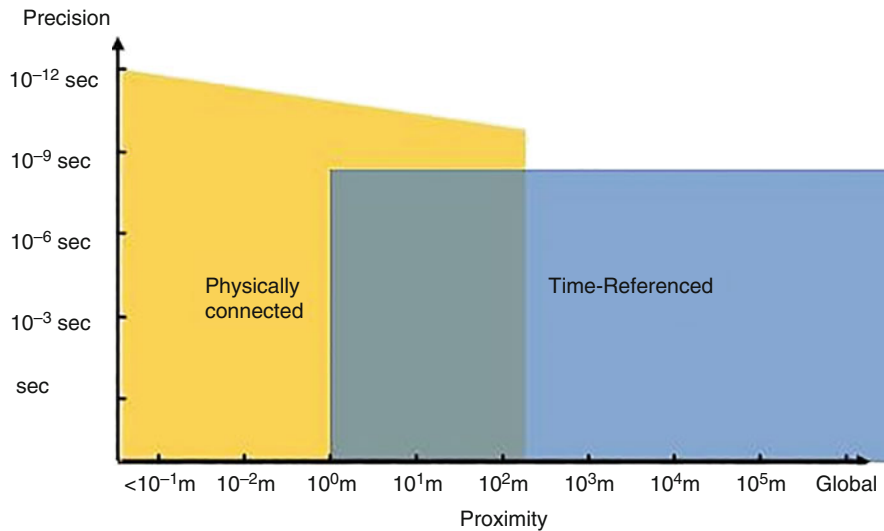


Fig. 17.2 Precision vs proximity of sensors with GPS time referencing [20]

The distance between sensors also affect the accuracy of such measurements. For physically connected systems, the proximity of the connection can increase the precision of the time measurement [20]. However, physical connections have their limits, and thus time-referenced synchronization approaches must be taken instead. However, various time synchronization methods result in different precision, and will be less accurate compared to when the sensors are physically connected (Fig. 17.2).

To summarize, factors to consider when time synchronization is attempted for vibration measurements include:

- Distance of sensors
- Frequency of interest
- Sampling rate of DAQ
- Amount of precision desired

17.3 Synchronization Algorithm

17.3.1 Theoretical Background – Analytic Signal and Real-Time Frequency

The Hilbert Transform $h(t)$ for a one-dimensional signal $x(t)$ is defined by the following integral:

$$h(t) = \frac{1}{\pi} \int_{-\infty}^{\infty} \frac{x(\tau)}{t - \tau} d\tau$$

The integral is improper and is evaluated as a Cauchy principal value. However, the transform may also be represented as a convolution:

$$h(t) = x(t) * y(t)$$

$$y(t) = \frac{1}{\pi t}$$

Performing a Fourier Transform on the above, the following is obtained:

$$H(\omega) = X(\omega) Y(\omega)$$

$$Y(\omega) = -i \operatorname{sgn}(\omega)$$

$$\text{sgn}(\omega) = \begin{cases} 1, & \omega > 0 \\ 0, & \omega = 0 \\ -1, & \omega < 0 \end{cases}$$

An Analytic Signal $x_a(t)$ of the signal $x(t)$ may be constructed using the Hilbert Transform:

$$x_a(t) = x(t) + ih(t)$$

After performing a Fourier Transform:

$$X_a(\omega) = X(\omega) + \text{sgn}(\omega) X(\omega)$$

This causes all the negative frequency components of $X(\omega)$ to cancel out, meaning $X_a(\omega)$ consists of solely the positive frequency components of $X(\omega)$. As a simple example, consider the following (note that A , ω , and ϕ are all functions of t , but the notation is omitted to limit clutter):

$$u(t) = A \cos(\omega t + \phi) = \frac{1}{2} \left(A e^{-i(\omega t + \phi)} + A e^{i(\omega t + \phi)} \right)$$

$$h_u(t) = \frac{1}{2} \left(i A e^{-i(\omega t + \phi)} - i A e^{i(\omega t + \phi)} \right)$$

$$u_a(t) = \frac{1}{2} \left(A e^{-i(\omega t + \phi)} + A e^{i(\omega t + \phi)} \right) + \frac{1}{2} i \left(A e^{-i(\omega t + \phi)} - i A e^{i(\omega t + \phi)} \right) = A e^{i(\omega t + \phi)}$$

Now, the phase of the analytic signal $u_a(t)$ can be extracted by taking its argument, which returns $\omega(t) \cdot t + \phi(t)$. If $\phi(t)$ varies slowly with time, then taking the derivative of the phase with respect to time will approximately give the Real-Time Frequency, which can easily be converted to Hz by dividing by 2π :

$$\frac{d[\omega(t)t + \phi(t)]}{dt} \approx \omega(t); f(t) = \frac{1}{2\pi} \omega(t)$$

The Real-Time Frequency obtained here is the main tool used to time synchronize separate readings of the voltage waveform from the power grid. This is discussed and explained in the next subsection. For a more in-depth discussion of the Hilbert Transform and the Analytic signal, see [21].

17.3.2 Outline of Algorithm

The algorithm developed as part of this study for time-synchronizing raw voltage waveform data from the power grid has multiple steps:

1. Compute the Real-Time Frequency (RTF) of the voltage waveforms
2. Split the first signal into several equally sized sub-sections
3. Calculate an initial time delay estimate (TDE) for each subsection of the first signal
4. Take the average of all the initial TDE's to obtain refined TDE
5. Apply correction due to phase offset between the signals

For ease of discussion, all data is assumed to be stored in column vectors. The subsample of the first signal will be referred to as sig1, its RTF referred to as rtf1, and its raw voltage waveform referred to as volt1. Likewise, for the second signal (i.e. sig2, rtf2, volt2). The associated time vector for sig1 will be referred to as time1, and time2 for sig2. Also, note that all the data collected was done so at 20,000 samples per second. The sampling frequency (20,000 samples/sec) will be referred to as f_s . sig1 is assumed to be completely contained within sig2 (that is, the data collection producing sig2 began before sig1, and the end of sig1 occurs before the end of sig2). Lastly, the algorithm discussed here assumes the raw voltage waveforms were measured under the same transformer (but perhaps on different phases). Other scenarios will be discussed at the end of this section.

17.3.3 Compute the Real-Time Frequency (RTF) of the Voltage Waveforms

The RTF's of sig1 and sig2 are computed by using the Hilbert Transform to obtain the Analytic Signal (see subsection A above). The Analytic Signals will be referred to as sig1A and sig2A, for sig1 and sig2 respectively. The Analytic Signal is of the form:

$$Ae^{i(\omega t + \phi)}$$

Where A is the amplitude, ω is the frequency in radians per second, and ϕ is some phase offset, which is assumed to vary slowly with respect to the period of the signal. The phase of the Analytic Signal, θ , is extracted from sig1A and sig2A, giving $\theta_1 = \omega_1 t + \phi_1$ for sig1A and $\theta_2 = \omega_2 t + \phi_2$ for sig2A. The derivative with respect to time of the phase is then computed to find the RTF (recall it is assumed ϕ varies slowly, so it can be treated as approximately constant), which is then divided by 2π to convert to Hertz:

$$f_1 = \frac{d\theta_1}{dt} * \frac{1}{2\pi} \approx \frac{\omega_1}{2\pi}$$

Note that to avoid discontinuous jumps caused by the phase, the unwrap function in MATLAB is used.

17.3.4 Split the First Signal into Several Equally Sized Sub-Sections

The length of the subsections should be at least 1 min long. As the frequency fluctuates, peaks and valleys are formed in the RTF plots. The algorithm uses these peaks and valleys to home in on regions that potentially correspond with the correct TDE (if this was not done, the runtime would be far larger). Testing revealed that sections of a minute or greater contain at least one peak or valley, but usually more.

17.3.5 Calculate an Initial Time Delay Estimate (TDE) for Each Subsection of the First Signal

“Magnitude of the Difference” (MoD) is next used to determine how well a particular shift of sig1 aligns with the corresponding portion of sig2 that has the same length as sig1, referred to as subSig2. The MoD was achieved by:

$$\text{abs} \left(\text{prctile} \left((\text{subSig2} - \text{sig1})^2, 15 \right) \right)$$

Where prctile() is a function in MATLAB. The first argument is a vector, in this case the square of the difference between subSig2 and sig1, and the second argument is the percentile to be returned. In this case, it was set to 15 (testing was done with several different percentiles, but the 15th percentile consistently provided a better result). The absolute value of this is then taken, as a smaller magnitude corresponds with two vectors being more alike. Taking the 15th percentile instead of the mean is beneficial, as this helps avoid outliers causing a bad result.

This operation can be used to test every possible shift of sig1; however, this is very inefficient, and often simply takes too long for larger datasets. To minimize the potential shifts investigated, the peaks and valleys of sig1 and sig2 are exploited. First, the two signals have their bias approximately removed, and then the magnitude is taken so that the valleys are now peaks as well:

$$\text{sig1M} = |\text{sig1} - \text{mean}(\text{sig1})| \text{ ssM}$$

$$\text{sig2M} = |\text{sig2} - \text{mean}(\text{sig1})|$$

The height of the first peak from sig1M is then used to find all peaks from sig2M that are within some threshold. A predetermined window is then used around these peaks, corresponding with all the shifts that the MoD should be calculated on. The smallest window that consistently gives good results is 1000 (indices) on either side of the peaks. The shift that corresponds with the MoD closest to zero is then taken to be the initial TDE.

17.3.6 Take the Average of All the Initial TDE's to Obtain Refined TDE

This is a straightforward step in the algorithm. A vector containing all initial TDE's from the previous step is formed, outliers are removed, and the mean is calculated. The implementation of removing outliers arose from test data occasionally having the end of sig1 end later than the end of sig2, causing there to not be a respective match for the last sub section of sig1. In the future, the algorithm should be made more robust to this, so it can recognize when there is no matching portion in sig2.

17.3.7 Apply Correction Due to Phase Offset Between the Signals

As stated previously, the raw voltage waveforms were assumed to be measured under the same transformer, but perhaps on different phases. Each phase of the power grid is 120° (a third of a period) off of the other two. This means to know the phase of one waveform relevant to another, the TDE acquired from the previous step must be within ~ 2.78 ms of the actual time delay (this corresponds with half of a third of a period). With this accuracy achieved, the TDE estimate can be corrected a great deal in this step, and the final TDE lies within two sample lengths of the true time delay (in the case of $f_s = 20,000\text{Hz}$). This translates to an uncertainty of ± 0.1 ms.

17.3.8 Other Scenarios

If the raw voltage waveforms were measured under the same transformer and on the same phase, then the algorithm above can be used to provide a TDE. If the raw voltage waveforms were measured in the same building, but different transformers, the algorithm outlined above will not provide a better estimate than part 4 can provide. When under different transformers, the relative phase offset between two waveforms may be any integer multiple of 30° , which would require an accuracy of ~ 0.7 ms. As of now, the algorithm is simply not accurate enough to resolve this, but research into improving and optimizing the algorithm may prove beneficial. The last scenario to discuss is raw voltage waveforms being taken over some long distance. In this case, the relative phase offset between the two signals could be anything, and so the accuracy here is limited by the accuracy of part 4 of the algorithm.

17.4 Methods

Modal analysis on a free-free beam test using the developed algorithm was performed to investigate the accuracy of the developed algorithm in different synchronization scenarios.

17.4.1 Free-Free Beam Modal Analysis

In this experiment, modal analysis is performed on a free-free aluminum beam using several different synchronization techniques. The first three operating deflection shapes (ODS) are extracted and compared with the theoretical Euler-Bernoulli beam model using MAC. By calculating the determinant of these MAC matrices, we can compare the accuracy of each synchronization method. This experiment was performed in the case of when the devices are on the same phase of the same transformer and when the devices are on different phases of the same transformer.

17.4.2 Experimental Setup

For the free-free beam setup, a 6061 Aluminum beam with dimensions 35.2 cm x 5.58 cm x 65024 cm was used. The beam tested was hung from two strings located at a fourth of the total length of the beam as measured from the left and right side of the beam. There were seven accelerometers on the beam, spaced equally from each other with an accelerometer at either

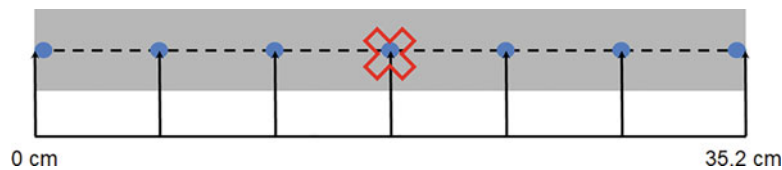


Fig. 17.3 Free-free beam setup

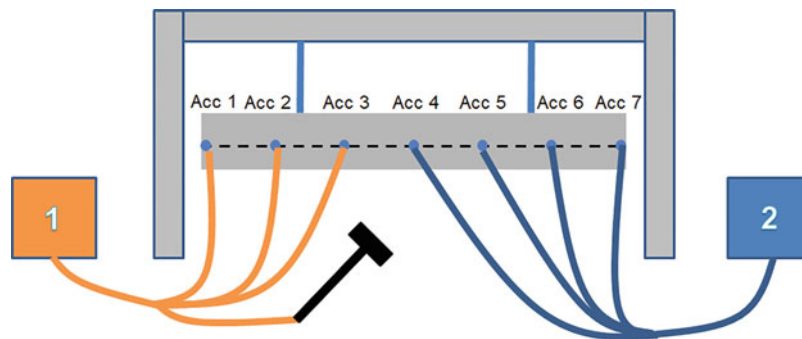


Fig. 17.4 General setup including DAQ cards

end of the beam. A modal testing hammer, Model 086C03 from PCB Piezotronics, was used to hit the center of the beam as indicated in Fig. 17.3 by the red 'X'. The numbers used to reference the accelerometers in the following section are labeled in Fig. 17.4.

For a general setup of the data acquisition hardware, two National Instruments PXI 1033 Chassis were used, each containing a National Instruments PXI 6683 Timing and Synchronization Module and several National Instruments PXI 4462 Sound and Vibration Modules. Based on the type of synchronization used, one or two DAQs would be used. The clocks used to time the sampling frequency would be based off of the PXI 6683 units, overriding the backplane clock of the PXI 1033 chassis. Data acquisition of the acceleration of the accelerometers and force of the hammer would then be acquired by LABVIEW.

17.4.3 Synchronization Testing Scenarios

The various synchronization techniques used which will be described later include:

1. No Synchronization
2. Pure Synchronization
3. Cable Synchronization
4. GPS Synchronization
5. Power Synchronization

In each synchronization scenario, the DAQ units were connected to the testing beam in different ways. The hammer, and the first three accelerometers were connected to one 4462 card (Card 1) while the other four accelerometers were connected to another 4462 card (Card 2). These were shifted around in accordance with various synchronization scenarios.

In addition, these experiments were run such that clock drift would be negligible with the exception of the No Synchronization scenario. This is done differently in each method which are described below.

In the first test scenario, No Synchronization, there was no synchronization between the two DAQ chassis. In this scenario, Card 1 and Card 2 are put on separate chassis, each individually timed by its own 6683 timing module. The free running 10 MHz temperature compensated crystal oscillators (TXCO) are used for the clock in each chassis. Then, during data acquisition, the two DAQs are turned on to acquire data in rapid succession by hand. This setup is a baseline case of where no attempt at robust synchronization is being done. This setup is seen in part a of Fig. 17.5.

In the second test scenario, Pure Synchronization, the two cards are connected to the same chassis, achieving the closest possible synchronization achievable with the equipment. In this scenario, both Card 1 and Card 2 are on the same chassis,

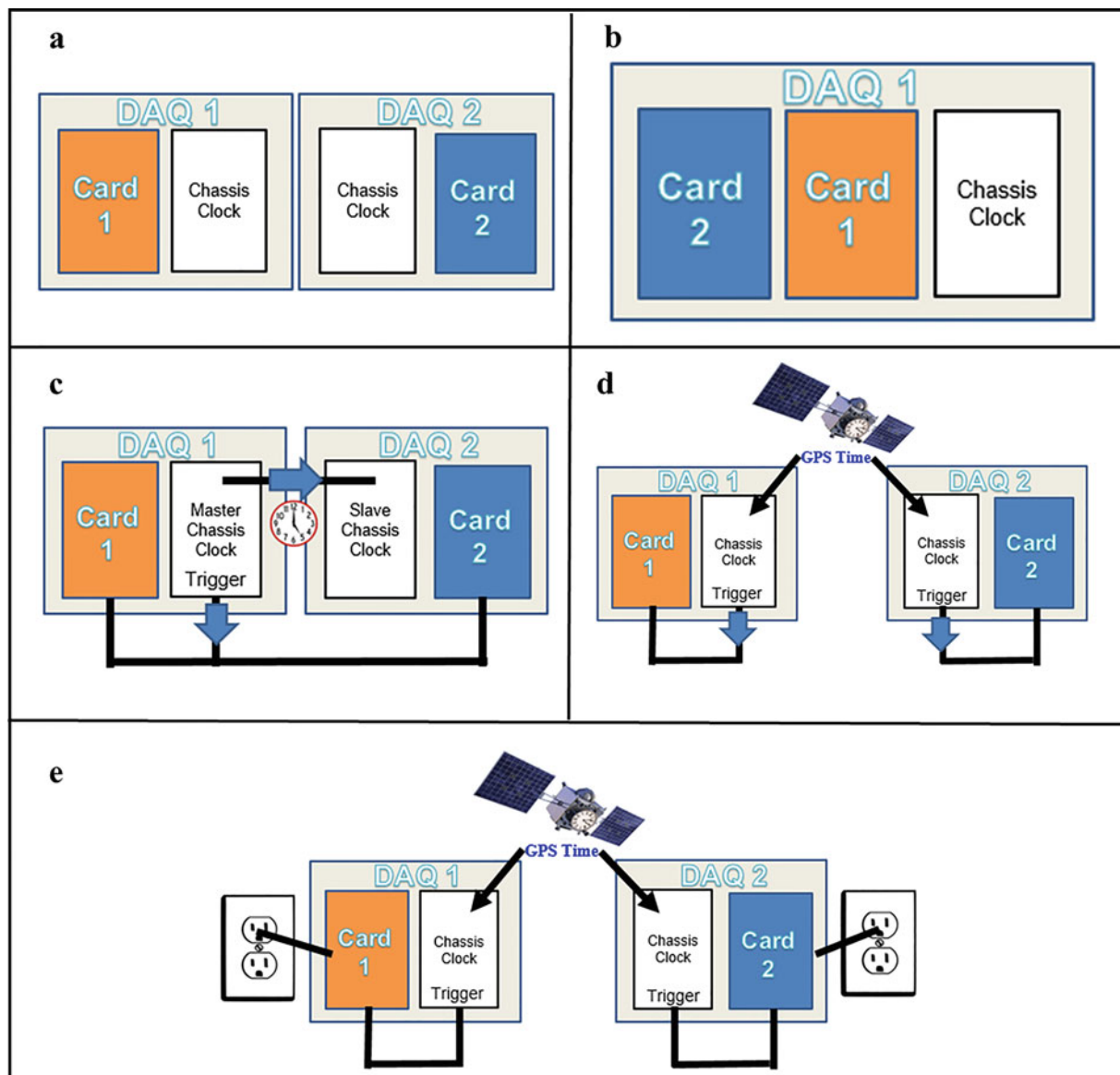


Fig. 17.5 Basic setup of all testing scenarios: a-No Synchronization, b-Pure Synchronization, c-Cable Synchronization, d-GPS Synchronization, e-Power Synchronization

which is timed by one of the modules. The 6683 module is using the TXCO, and since its clock is sent synchronously to both cards, both cards are synchronized with each other, with both cards having no clock skew or clock drift. During data acquisition, the chassis would be turned on to acquire data for both cards at the same time. This setup is seen in part b of Fig. 17.5.

In the third test scenario, Cable Synchronization, the two cards are on two separate DAQ chassis. In this scenario, the clocks of each 6683 card on each chassis is connected through a synchronization cable. The master chassis with Card 1 has a master clock that sends its clock over to the slave clock in the chassis with Card 2. There is also a trigger on the chassis with Card 1 that is sent to both DAQ units, causing them to start at the same time when the trigger is sent. As a result, the data acquisition is synchronized and started at the same time when one chassis is turned on. This results in no clock drift or clock skew. This setup is seen in part c of Fig. 17.5.

The fourth test scenario, GPS Synchronization, also has the two cards on two separate chassis. However in this scenario, the clocks of each 6683 card on each chassis are disciplined to a GPS clock. This is done by connecting a Trimble Bullet GPS Antenna to the 6683 chassis, ensuring that the antenna has a clear line of sight to the sky. The 6683 modules send a trigger to the 4462 acquisition cards at a set time, resulting in synchronous activation and allowing both DAQs to be synchronized

to the GPS clock. The clocks are sampling their frequencies according to the GPS clock, thereby resulting in no clock drift. This setup is seen in part d of Fig. 17.5.

The fifth test scenario, Power Synchronization, is the synchronization method this paper is comparing to the other synchronization methods. In this case the two cards are on two separate chassis. In addition to recording the sensors on the cards, the chassis are also recording the power of the grid by a LeCroy AP031 Differential Probe. This power grid data will be used to acquire the correct time delay using the algorithm mentioned in sect. III. To start the two DAQs, these DAQ units are connected to the GPS clock, which triggers each DAQ at separate times. The DAQs are still connected to the GPS clock to prevent clock drift. This is also done so that when the algorithm is used, there can be a comparison between the time delay the algorithm calculates and the time delay calculated by the GPS clock. The actual power synchronization algorithm does not use the GPS clock for time skew. This setup is seen in part e of Fig. 17.5.

This test scenario is done twice, once where the devices are connected to the same phase of the power grid, and different phases of the power grid, resulting in a total of 6 test scenarios:

1. No Synchronization
2. Pure Synchronization
3. Cable Synchronization
4. GPS Synchronization
5. Power Synchronization (Same Phase)
6. Power Synchronization (Different Phase)

17.4.4 Experiment Procedure

To acquire the ODS of the beam with the various synchronization techniques, 3 trial runs of 6 continuous hits on the beam were performed with the modal hammer. These were taken each at 10 second intervals. However, for Power Synchronization, since more time is required to align the power signals, there was a wait period after beam tests where the DAQ acquires voltage data. This was 5 minutes in the case of same phase, and 20 minutes long in the case of different phase.

17.5 Data Analysis

In order to convert the collected vibrational data from the accelerometers to interpretable ODS, a MATLAB code was used to analyze the accelerometer data.

The FRF was created from dividing the Fourier transform of the output (accelerometer data) over the input (force sensor on hammer data). The peaks of the FRF were then identified to find the resonant frequencies. The ODS were found at the corresponding resonant frequencies. These were then compared to the analytical mode shapes by using a MAC matrix. The analytical mode shapes were calculated using the free vibration equation for a free-free Euler-Bernoulli beam.

To compare the MAC matrices from several trials of each time-synchronization technique, the determinant, along with its mean and standard deviation, was calculated for each MAC matrix (Fig. 17.6).

17.6 Results

In order to compare the accuracies of each synchronization method, and how well each one would fare in a real vibration test, a MAC matrix was used to compare the analytical results derived from the Euler-Bernoulli beam equation to the ODS extracted from the experiment using the various synchronization methods. This was done for all six synchronization scenarios tested, Table 17.1.

According to the calculations derived from the Euler-Bernoulli beam equations, the modes were calculated to be 287.3, 791.9, and 1552.5 Hz. The FRF from the pure synchronization experiment is shown in Fig. 17.7 and the values agree within 10% of the analytically calculate resonant frequencies.

In order to condense this information, the determinants of the MAC matrices were graphed as a bar chart (Fig. 17.8):

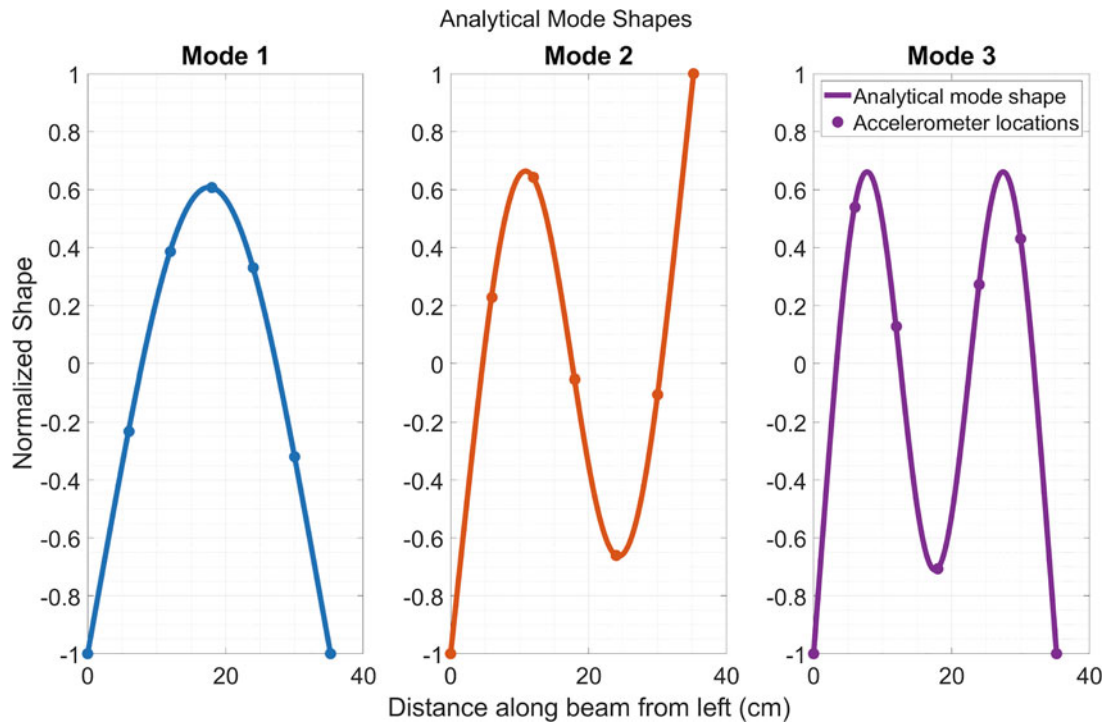


Fig. 17.6 Analytical mode shapes

Table 17.1 MAC matrix determinant values of each synchronization method

Sync method	MAC matrix determinant	Uncertainty (2 standard deviations)
No synchronization	-0.0003967	0.00206
Pure synchronization	0.9316	0.002945
Cable	0.9341	0.0007062
GPS	0.9294	0.0005945
Power (same phase)	0.9202	0.0042525
Power (different phase)	0.9193	0.05051

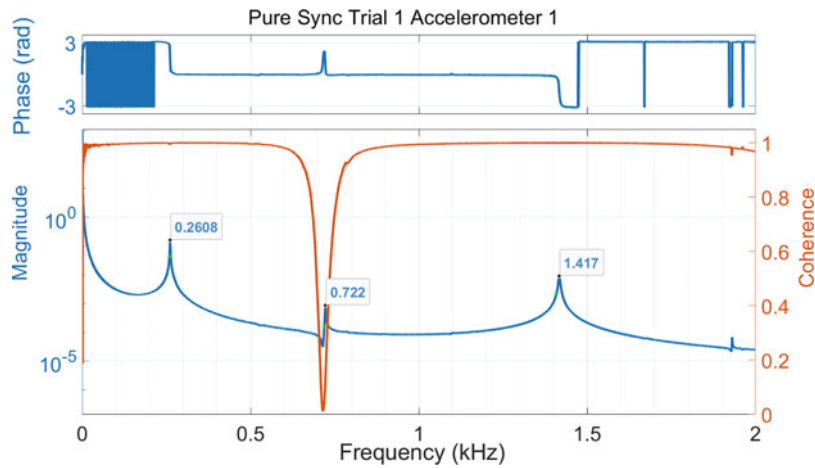


Fig. 17.7 Experimental resonant frequencies in FRF from Pure Synchronization Trial 1

All the resulting MAC matrices, other than No Synchronization, have diagonals that are closely related to 1. In order to compare the MACs with each other, the determinant of each matrix was taken. If the determinants were 1, the vectors would be correlated. If the determinants were 0, the vectors would be uncorrelated.

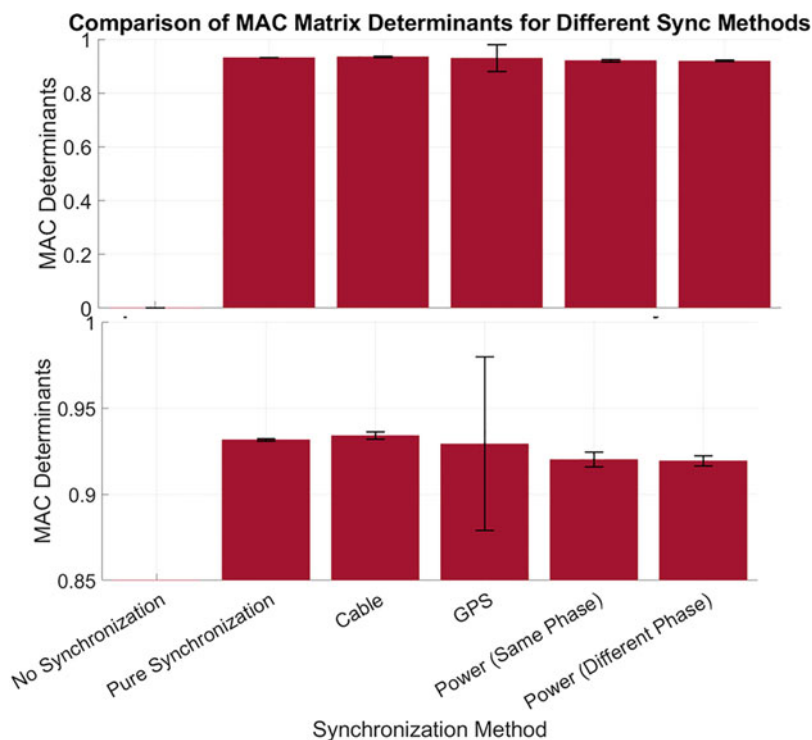


Fig. 17.8 MAC Matrix Comparison Bar Graph (Top shows full graph, bottom zooms into upper portion of graph)

As seen above, the Power Sync MAC matrices have determinants that are very close to 1 alongside with the MAC matrices of traditional synchronization techniques. This shows that for this test case, power synchronization is comparable to traditional synchronization methods with this algorithm when the devices are connected to the same phase and different phases.

This can also be seen by comparing the ODS directly to the analytical solution. The analytical modes are compared to the ODS acquired from power synchronization in Figs. 17.9 and 17.10. As seen in those figures, the shapes agree closely.

17.7 Conclusions

This paper presents a novel form of synchronization through power grid measurements. This new approach expands on the ease of access of synchronization without specialized equipment and with less restrictions on the environment of synchronization. This synchronization method is compared to other traditional synchronization methods by comparing MAC matrices gathered on a free-free beam modal analysis experiment.

The algorithm developed in this paper was shown to perform accurately alongside with traditional forms of synchronization under cases of same phase and different phase on the same transformer network. The power synchronization algorithm was able to produce comparatively similar MACs to traditional synchronization methods alongside the theoretical modes of the beam. The ODS acquired for the power synchronization method, just like when gathered from traditional synchronization methods, are very similar to theoretical mode shapes derived from Euler Bernoulli beam theory.

This experiment is under the assumption that the power grid is consistent and provides continuous power and is resilient to failures. There are anomalies such as swell, undervoltage, sag, and interruptions. More studies need to be performed under the case where power grid voltage data is not always consistently there.

In addition, this experiment was conducted when all clocks were sampling at exactly the same frequency. Because clock drift always occurs when clocks are not connected to a common clock, further investigation needs to be done on how the power synchronization algorithm fare when clock drift is introduced.

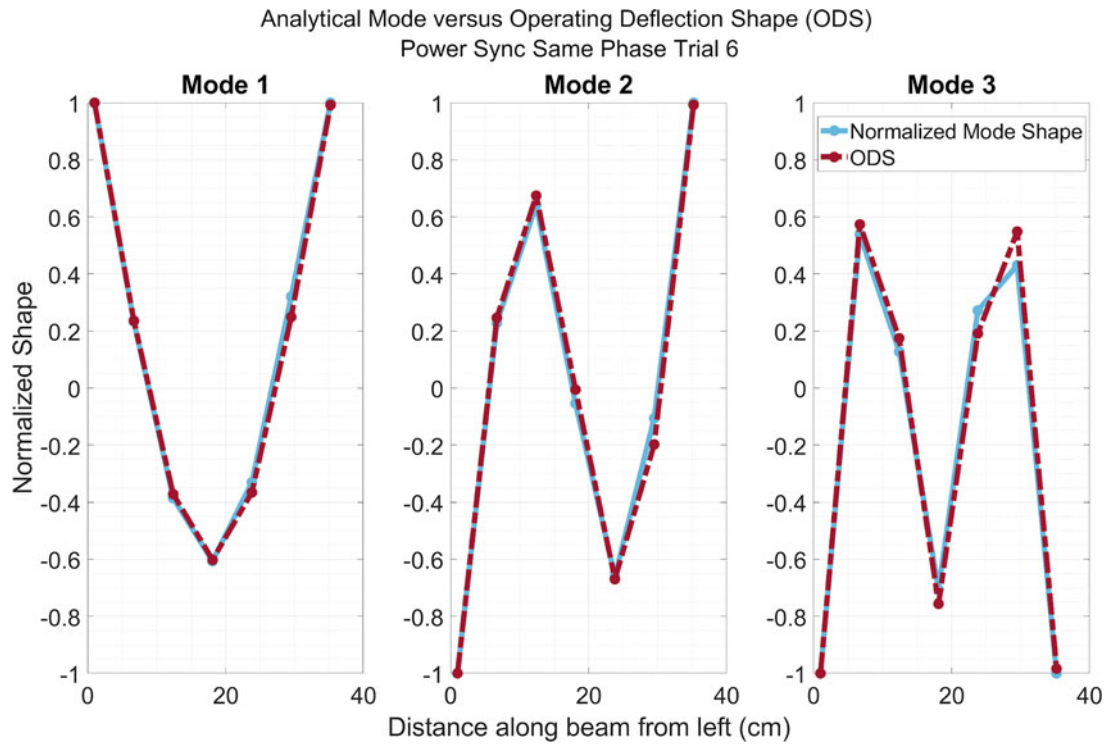


Fig. 17.9 Analytical mode versus ODS in Power Sync Same Phase Trial 6

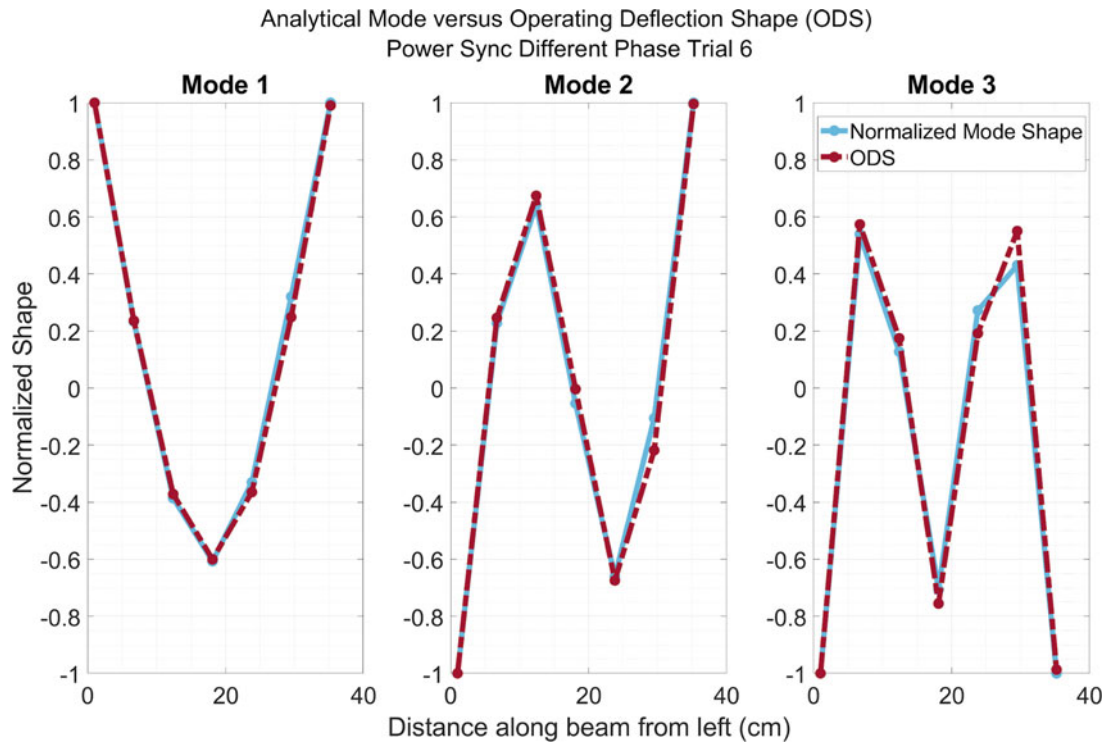


Fig. 17.10 Analytical mode versus ODS in Power Sync Different Phase Trial 6

Appendix

Table 17.2 Pure synchronization modal assurance criterion matrix

Theoretical	Analytical mode shapes		
	1	2	3
1	0.9973 ± 0.0000	0.0005 ± 0.000	0.2583 ± 0.0002
2	0.00015 ± 0.0002	0.9942 ± 0.003	0.001217 ± 0.0020
3	0.2061 ± 0.0002	0.0012 ± 0.000	0.9929 ± 0.0000

Table 17.3 No synchronization modal assurance criterion matrix

Theoretical	Analytical mode shapes		
	1	2	3
1	0.01727 ± 0.02	0.1446 ± 0.2	0.1684 ± 0.2
2	0.02135 ± 0.04	0.0259 ± 0.05	0.08115 ± 0.2
3	0.02633 ± 0.06	0.05478 ± 0.04	0.1881 ± 0.2

Table 17.4 Cable synchronization modal assurance criterion matrix

Theoretical	Analytical mode shapes		
	1	2	3
1	0.9978 ± 0.0001	0.0002667 ± 0.0001	0.2532 ± 0.0007
2	0.0007833 ± 0.0004	0.9942 ± 0.0004	0.00008333 ± 0.0002
3	0.199 ± 0.001	0.002067 ± 0.001	0.992 ± 0.0004

Table 17.5 GPS synchronization modal assurance criterion matrix

Theoretical	Analytical mode shapes		
	1	2	3
1	0.9973 ± 0.0000	0.0004833 ± 0.00008	0.2664 ± 0.0003
2	0.0008167 ± 0.0010	0.9943 ± 0.00070	0.0001333 ± 0.0002
3	0.2081 ± 0.0002	0.001967 ± 0.00020	0.9928 ± 0.0001

Table 17.6 Power synchronization (same phase) modal assurance criterion matrix

Theoretical	Analytical mode shapes		
	1	2	3
1	0.9976 ± 0.0002	0.0002 ± 0.0002	0.2628 ± 0.002
2	0.0003833 ± 0.001	0.9948 ± 0.001	0.0003 ± 0.0005
3	0.2089 ± 0.008	0.004067 ± 0.003	0.9914 ± 0.001

Table 17.7 Power synchronization (different phase) modal assurance criterion matrix

Theoretical	Analytical mode shapes		
	1	2	3
1	0.9975 ± 0.0005	0.0001833 ± 0.0003	0.2626 ± 0.004
2	0.0005 ± 0.0007	0.9947 ± 0.0004	0.00015 ± 0.0003
3	0.2154 ± 0.04	0.01065 ± 0.04	0.9832 ± 0.04

References

1. Balageas, D.: Introduction to structural health monitoring. (2006)
2. Xiong, C., et al.: Operational modal analysis of bridge structures with data from GNSS/accelerometer measurements. *Sensors*. **17**, 436 (2017). <https://doi.org/10.3390/s17030436>
3. Kim, R., Nagayama, T., Jo, H., & Spencer, B.: Preliminary study of low-cost GPS receivers for time synchronization of wireless sensors. *Proceedings of SPIE – The International Society for Optical Engineering*. 31. (2012). <https://doi.org/10.1117/12.915394>
4. The U.S. electric system: A complex, interdependent network. Retrieved from https://www.eia.gov/realtime_grid/#/summary/about?end=20190403&start=20190327
5. Fonville, B., Matsakis, D., & Hardis, J.: Time and frequency from electrical power lines. (2017). <https://doi.org/10.33012/2017.14996>
6. Viswanathan, S., Tan, R., & Yau, D. K. Y.: Exploiting power grid for accurate and secure clock synchronization in industrial IoT. (2016). <https://doi.org/10.1109/RTSS.2016.023>
7. Rowe, A., Gupta, V. & Rajkumar, R.: Low-power clock synchronization using electromagnetic energy radiating from AC power lines. *Proceedings of the 7th ACM Conference on Embedded Networked Sensor Systems, SenSys 2009*. pp. 211–224. (2009). <https://doi.org/10.1145/1644038.1644060>
8. Avitabile, P.: Modal testing. (2018)
9. Chandravanshi, M & Mukhopadhyay, A: Modal Analysis of Structural Vibration. (2013). <https://doi.org/10.1115/IMECE2013-62533>
10. Synchronization Basics. (n.d.). Retrieved from <https://www.ni.com/en-us/innovations/white-papers/12/synchronization-basics.html>
11. Comparing Signal-Based and Time-Based Synchronization. (n.d.). Retrieved from <http://zone.ni.com/reference/en-XX/help/373629D-01/nisync/v/compare-signal-vs-time-programming/>
12. Young Koo, K., Hester, D., Kim, S.: Time synchronization for wireless sensors using low-cost GPS module and Arduino. *Front. Built Environ.* **4**, (2019). <https://doi.org/10.3389/fbuil.2018.00082>
13. Lombardi, M., Nelson, L.M., Novick, A.N., Zhang, V.: Time and frequency measurements using the global positioning system. *Cal Lab Int. J. Metrol.* **8**, 26–33 (2001)
14. Li, L. et al.: Exploiting FM radio data system for adaptive clock calibration in sensor networks. *MobiSys*, (2011)
15. Hao, T., Zhou, R., Xing, G., Mutka, M.W.: WizSync: exploiting Wi-fi infrastructure for clock synchronization in wireless sensor networks. *IEEE Trans. Mobile Comput.* **13**, 149–158 (2011). <https://doi.org/10.1109/RTSS.2011.21>
16. Li, Zhenjiang, Chen, Wenwei, Li, Cheng, Li, Mo, Li, Xiang-Yang & Liu, Yunhao. FLIGHT: clock calibration using fluorescent lighting. (2012) <https://doi.org/10.1145/2348543.2348584>
17. Björklund, S., Le, G. & Nil, R.: A survey and comparison of time-delay estimation methods in linear systems. (2019)
18. Correlation. Retrieved from http://www.ee.ic.ac.uk/hp/staff/dmb/courses/E1Fourier/00800_Correlation.pdf
19. Bocca, M., Eriksson, L., Mahmood, A., Jantti, R., Kullaa, J.: A synchronized wireless sensor network for experimental modal analysis in structural health monitoring. *Comp. Aided Civil Infrastruct. Eng.* **26**, 483–499 (2011). <https://doi.org/10.1111/j.1467-8667.2011.00718.x>
20. Timing and Synchronization Systems. (2019). Retrieved from <http://www.ni.com/product-documentation/9882/en/>
21. Hahn, S.L.: Chapter 7: Hilbert transforms. In: Poularakis, A. (ed.) *The Transforms and Applications Handbook*. CRC Press, Boca Raton (1996)